J. Membrane Biol. 32, 255–290 (1977)

K^+ Conduction Description from the Low Frequency Impedance and Admittance of Squid Axon

H. M. Fishman*, D. J. M. Poussart**, L. E. Moore*, and E. Siebenga***

Marine Biological Laboratory, Woods Hole, Massachusetts 02543

Received 18 March 1976; revised 28 July 1976

Summary. The form of power spectra of K^+ conduction fluctuations in patches of squid axon suggested that K^+ conduction kinetics are higher than first order (Fishman, Moore & Poussart, 1975, *J. Membrane Biol.* **24**:305). To obtain an alternative description of ion conduction kinetics consistent with spontaneous fluctuations, the complex impedance and admittance of squid (*Loligo pealei*) axon were measured at low frequencies (1–1000 Hz) with a four electrode system using white Gaussian noise as a stochastic perturbation. As predicted from the spontaneous noise measurements, a low frequency impedance feature is observed between 1 and 30 Hz which is voltage and temperature dependent, disappears after substantial reduction in $[K_i^+]$, and is unaffected by the state of Na^+ conduction or active transport. These measurements confirm and constitute strong support for the patch noise measurements and interpretations. The linearized Hodgkin-Huxley (*HH*) equations do not produce the low frequency feature since first order ion conduction kinetics are assumed. Computation of diffusion polarization effects associated with the axon sheath gives a qualitative account of the low frequency feature, but the potential dependence is opposite to that of the data. Thus, K^+ conduction kinetics in the axon are not adequately described by a single first order process. In addition, significant changes in *HH* parameter values were required to describe the usual impedance (resonance) feature in *Loligo pealei* axon data.

Spectral analysis of spontaneous current fluctuations in small patches (Fishman, 1973*a*; Fishman, Moore & Poussart, 1975), as well as in large areas (Conti, DeFelice & Wanke, 1975) of squid axon membrane, indicate that noise at rest and depolarized membrane potentials contains a dominant component which relates to potassium-ion conduction. Based upon the low and high frequency asymptotic behavior of the spectra, which was ostensibly flat at low frequencies and declined with a logarithmic slope of 2 at high frequencies, the phenomenon producing this K^+ noise com-

* *Permanent address and for reprint requests:* Department of Physiology and Biophysics, University of Texas Medical Branch, Galveston, Texas 77550.

** *Permanent address:* Laboratoire de Bionique, Département de Génie Electrique, Université Laval, Québec, Canada.

*** *Permanent address:* Department of Physiology, University of Leiden, Leiden, The Netherlands.

ponent was tentatively identified as a relaxation (first order kinetics) process. However, the form of current noise spectra in small patches in the transition (from low to high frequency) region was significantly sharper than that of a first order rate process, implying that the K^+ conduction kinetics are of higher order (Fishman, Moore & Poussart, 1975). In order to confirm this finding, an alternative means of clarifying the noise measurements was sought.

A basic difficulty in comparing spontaneous noise data with data from step voltage clamp experiments is that noise data are derived from experiments which involve small-amplitude spontaneous fluctuations during steady-state conditions whereas voltage clamp data are usually obtained for large signal, transient perturbations. Since membrane conduction is grossly nonlinear, a comparison under widely different signal levels and temporal conditions is inappropriate. A more suitable comparison would be between the response to small signal steady-state perturbations and spontaneously generated membrane noise. The major existing data, in this respect, are the complex impedance measurements of Cole (1968) and collaborators. These measurements, which covered the range from 10 Hz to 10 kHz, were longitudinal, produced membrane potential changes of only a few mV and required removal of the cable impedance in order to describe the membrane linear properties. In the thirty or more years since Cole's original measurements, complex impedance has been neglected as a useful means of acquiring membrane conduction information. The few experiments which have been reported have focused primarily on high frequency aspects where the membrane capacitance dominates the impedance (Taylor, 1965; Matsumoto, Inoue & Kishimoto, 1970; Takashima & Schwann, 1974; Takashima, Yantorno & Pal, 1975; Takashima, Schwann & Cole, 1975). The lack of interest in impedance during this period can be attributed mainly to the success of potential control experiments in the description of ion conduction and the limited type of experiments which could be conducted because of the lengthy data-acquisition intervals required in ac bridge measurements.

A contemporary alternative to bridge measurements of complex impedance is a method (Fishman, 1975) which uses "white" noise as a stochastic signal to obtain the membrane response at all frequencies of interest (Lee, 1960; Davies, 1970). This method has three important advantages: (1) it provides rapid and detailed measurement of complex impedance, (2) it provides reliable data in the presence of substantial extraneous noise, (3) it facilitates use of four electrodes which minimize electrode polarization effects and extends measurements to low frequencies.

The impedance information is obtained from cross-correlation of current-noise input with membrane-potential output and conversion to the real and imaginary parts of the complex impedance by Fourier transformation. In addition to the measurements described here, applied noise has also been used by Dr. Rita Guttman and colleagues (Guttman, Feldman & Lecar, 1974; Guttman & Feldman, 1975).

These experiments arose from the use of spectra of spontaneous K^+ conduction noise to modify and evaluate the element values contained in a circuit realization of the linearized Hodgkin-Huxley description of potassium and leakage conduction. Computation of the complex impedance of the circuit with the parallel addition of membrane capacitance suggested a low frequency feature which had not been reported. Our impedance measurements[1] confirmed the existence of this feature which is potential, temperature, and K^+ current dependent but not associated with Na^+ current or active transport. These results are thus consistent with and are strong support for the patch noise data. The noise data suggest that K^+ conduction kinetics are not first order. Furthermore, the finding of significant differences in conduction parameters for Woods Hole axons from those in the Hodgkin-Huxley formulation suggests that applied noise measurements of complex impedance or admittance can provide an alternative, detailed description of ion conduction with the speed and accuracy which is necessary for evaluation of kinetic models.

Ion Conduction Description from the Linearized Hodgkin-Huxley (ℓHH) Equations

As a basis for discussion and comparison with experimental data, an expression for the admittance of an axon membrane is obtained by linearizing the *HH* equations (Chandler, FitzHugh & Cole, 1962; Mauro, Conti, Dodge & Schor, 1970). The resulting complex ($p=j\omega$) admittance is

$$Y(p)=Cp+g_\infty+\frac{g_n}{1+p\tau_n}+\frac{g_m}{1+p\tau_m}+\frac{g_h}{1+p\tau_h} \tag{1}$$

where[2]

1 Preliminary accounts of these measurements were given previously (Fishman, 1975; Fishman, Moore, Poussart & Siebenga, 1976).

2 The convention used is that V's are displacements from rest potential with a positive value indicating a depolarization.

$$
\begin{aligned}
&g_\infty = \bar{g}_K n_\infty^4 + \bar{g}_{Na} m_\infty^3 h_\infty + g_L \\
&g_n = 4\bar{g}_K n_\infty^3 \tau_n (V - V_K)\,[\alpha_n' - n_\infty(\alpha_n' + \beta_n')] \\
&g_m = 3\bar{g}_{Na} m_\infty^2 h_\infty \tau_m (V - V_{Na})\,[\alpha_m' - m_\infty(\alpha_m' + \beta_m')] \\
&g_h = \bar{g}_{Na} m_\infty^3 \tau_h (V - V_{Na})\,[\alpha_h' - h_\infty(\alpha_h' + \beta_h')]
\end{aligned} \tag{1a}
$$

$$
\tau_n = (\alpha_n + \beta_n)^{-1} \qquad \tau_m = (\alpha_m + \beta_m)^{-1}, \qquad \tau_h = (\alpha_h + \beta_h)^{-1}
$$

$$
n_\infty = \alpha_n \tau_n, \qquad m_\infty = \alpha_m \tau_m, \qquad h_\infty = \alpha_h \tau_h,
$$

$$
\begin{aligned}
&\alpha_n = 0.1 f(1 - 0.1\,V)\,T_f \\
&\beta_n = 0.125 \exp(-V/80)\,T_f \\
&\alpha_m = f(2.5 - 0.1\,V)\,T_f \\
&\beta_m = 4 \exp(-V/18)\,T_f \\
&\alpha_h = 0.07 \exp(-V/20)\,T_f \\
&\beta_h = [1 + \exp(3 - 0.1\,V)]^{-1}\,T_f
\end{aligned} \tag{1b}
$$

$$
f(x) = \frac{x}{\exp(x) - 1}
$$

$$
T_f = Q_{10}[(T - 6.3)/10]
$$

and

$$
\begin{aligned}
&\alpha_n' = \frac{d\alpha_n}{dV} = -0.01 f'(1 - 0.1\,V)\,T_f \\
&\beta_n' = -\beta_n/80 \\
&\alpha_m' = -0.1 f'(2.5 - 0.1\,V)\,T_f \\
&\beta_m' = -\beta_m/18 \\
&\alpha_h' = -\alpha_h/20 \\
&\beta_h' = 0.1\,\beta_h^2 \exp(3 - 0.1\,V)/T_f \\
&f' = [\exp(x) - 1 - x \exp(x)]\,[\exp(x) - 1]^{-2}.
\end{aligned} \tag{1c}
$$

The *HH* values are $V_K(-12\,\text{mV})$, $V_{Na}(115\,\text{mV})$, $V_L(10.6\,\text{mV})$, $\bar{g}_K(36\,\text{mmho/cm}^2)$, $\bar{g}_{Na}(120\,\text{mmho/cm}^2)$, $g_L(0.3\,\text{mmho/cm}^2)$ and $Q_{10}(3)$. From Eq. (1) a circuit synthesis of the admittance is apparent as a parallel combination of branches corresponding to each of the 5 terms in the admittance. In Fig. 1*a*, a circuit is drawn so that the branches which correspond to each ion conduction process are grouped together. g_∞, the chord con-

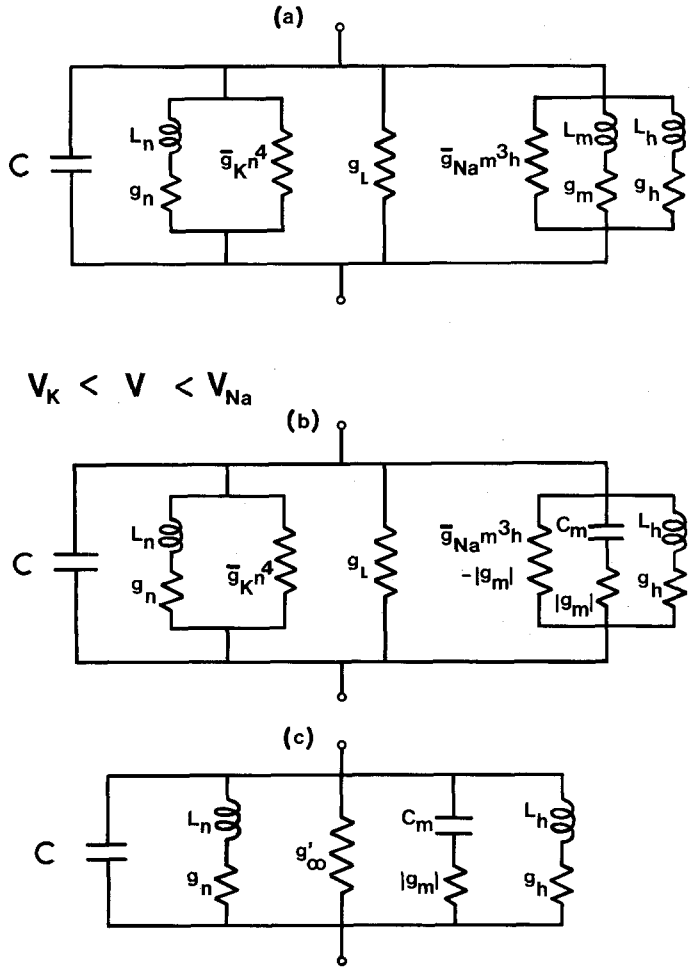

Fig. 1. Electrical circuit description of axon small signal behavior from the linearized Hodgkin-Huxley equations. (*a*) Circuit realization of the admittance Y in Eq. (1). The chord conductance g_∞ has been split into three parallel branches and grouped with branches corresponding to specific ion conduction processes. (*b*) In the normal potential range $V_K < V < V_{Na}$, g_m and L_m have negative values and can be converted to a $|g_m|$ and C_m, which have positive values, with an additional term $-|g_m|$ added to the chord conductance for the Na^+ process. (*c*) Condensation of circuit in (*b*) in which g'_∞ is the parallel combination of chord conductances from all conduction processes. Note that without Na^+ conduction ($\bar{g}_{Na}=0$) $g'_\infty = \bar{g}_K n^4 + g_L$ and $|g_m|$ C_m and $g_h L_h$ branches are omitted. Without K^+ conduction ($\bar{g}_K=0$) $g'_\infty = \bar{g}_{Na} m^3 h + g_L - |g_m|$ and $g_n L_n$ branch is omitted

ductance, has been split into three parallel conductances to show the contribution to the circuit from each of the conduction processes. The capacitance C and leakage conductance g_L are the only elements assumed to be independent of voltage and are taken be $1\,\mu F/cm^2$ and $0.3\,mmho/cm^2$.

All other elements have fixed values only under the condition of constant voltage. Note that the frequency dependence of the n, m and h processes is represented by (gL) branches consisting of a conductance in series with an inductance. The g's are given by Eq. (1*a*) and the L values can be obtained from the relation $\tau_i = g_i L_i$ for each of the processes. In the usual range of membrane potential ($V_K < V < V_{Na}$) $g_m < 0$ and since $\tau_m > 0$, then $L_m = \tau_m / g_m < 0$. The $g_m L_m$ branch in Fig. 1*a*, which has negative element values, can be converted to a $g_m C_m$ branch, which has positive element values, by changing the Na^+ chord conductance (Chandler *et al.*, 1962; Mauro *et al.*, 1970). In the transformation, the time constants must be equal. Thus for $V < V_{Na}$

$$\tau_m = g_m L_m = -C_m/g_m = C_m/|g_m| > 0$$

and

$$C_m = -g_m^2 L_m > 0,$$

where the absolute value of g_m is used in the transformed circuit of Fig. 1*b* and 1*c* to obtain a positive conductance and to give $\tau_m > 0$. Furthermore, the behavior at all frequencies must remain the same. This is achieved by the addition of a parallel $-|g_m|$ branch to the $|g_m|$ C_m branch (in Fig. 1*b*) which together have the same admittance function as the $g_m L_m$ branch they replace. The equivalence of the two circuits is obvious at zero and infinite frequency. The change from negative inductance to positive capacitance is made to emphasize that the m process, in the normal potential range, behaves as a reactance which can resonate with the inductive reactances from the n and h processes. The entire circuit can then be simplified into 5 parallel branches in Fig. 1*c*, where $g'_\infty = g_\infty - |g_m|$.

Eq. (1) and the subsequent parameter defining equations were programmed for solution on a PDP 11/40 computer. The complex admittance $Y(j\omega)$ could be calculated for the standard HH values, given previously, as well as for changes in any parameter. A parallel $g_s \| C_s$ admittance Y_s was added in series with the HH Y [Eq. (1)], to account for experimental conditions, to give a total admittance

$$Y_T = \frac{YY_s}{Y + Y_s}.$$

The complex impedance was calculated as a reciprocal of Y_T from which the magnitude $|Z|$ and phase ϕ were calculated and plotted as functions of frequency.

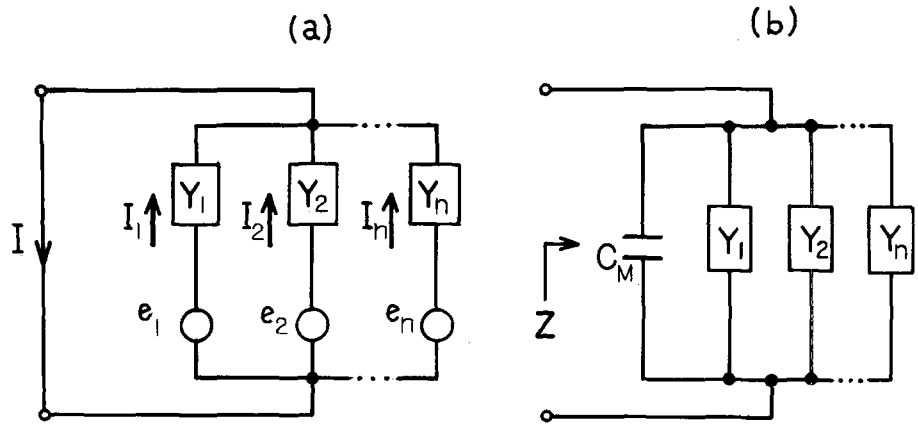

Fig. 2. (*a*) Generalized circuit (linearized) description of ion conduction under conditions of (1) maintained constant voltage between circuit terminals and (2) uncorrelated white-noise voltage sources (*e*'s) in series with each branch admittance. The measured power spectrum $S_I(f)$ of fluctuations in I may be used to identify the branches and elements as described in text. (*b*) The complex impedance can be computed from the circuit established in (*a*) by addition of a parallel (membrane) capacitance. The computation can then be compared with measurements of $|Z|$ and ϕ as a function of frequency

Determination of Membrane Impedance from Noise Data

The method described here is an extension of passive, linear circuit theory. A circuit realization of conduction similar to the ℓHH circuit (Fig. 1*c*) is assumed in the form of a parallel combination of simple branches (Fig. 2*b*), each of which consists of either a resistance R, capacitance C, inductance L, series RL, series RC or series RLC. Although consideration of only these types of branches appears restrictive, it can be shown that parallel combinations of these types can yield reasonable approximations to rather complicated impedance functions.

Under equilibrium conditions, only the resistive element in any branch produces (thermal-white) noise given by the Nyquist (1928) relation. For the purpose of noise analysis, then, the behavior can be obtained from a circuit containing noiseless elements with thermal voltage noise sources in series with each branch resistance. The spectrum of current noise, measured over all frequencies and under constant voltage conditions, from the assumed circuit (Fig. 2*a*) gives the frequency dependence of the individual branches and the intensities of the various thermal sources. Under nonequilibrium conditions, it is assumed that excess noise generation is also associated with the dissipative elements and that the noise power is uniformly distributed (white) in the measured frequency range.

That is, the thermal noise sources can be replaced by white noise sources with intensities which exceed the thermal levels. Measured spectral features permit identification of those branches which contribute significant noise to the measurement. This latter extension from the equilibrium to the nonequilibrium case appears reasonable since, for example, shot noise would approximate an excess white noise at low frequencies. However, noisy processes such as f^{-1} phenomena, which do not conform to the fluctuation-dissipation theorem (Kubo, 1957), are excluded from this type of analysis.

The above method is first described for two trivial cases which are subsequently used to fit a measured potassium-ion current noise spectrum, $S_{I_K}(f)$. Consider, first, the case of a single series circuit consisting of an RL in series with a white-noise voltage source S_e. The squared magnitude of admittance is

$$|Y|^2_{RL} = R^{-2} F_{RL}(f) \tag{2.0}$$

where

$$F_{RL}(f) = [1 + (f/f_c)^2]^{-1} \tag{2.0a}$$

and

$$f_c = (2\pi L/R)^{-1}.$$

The current-noise power spectrum is

$$S_I(f) = |Y|^2_{RL} S_e(f). \tag{2.1}$$

Since the voltage noise source is assumed to be white, $S_e(f) = S_{e_0}$ (a constant), and

$$S_I(f)/S_{e_0} = |Y|^2_{RL}. \tag{2.2}$$

Since R in Eq. (2.0) is also constant, a new constant is defined

$$S_0 = R^{-2} S_{e_0}$$

and

$$S_I(f)/S_0 = F_{RL}(f). \tag{2.2a}$$

Consequently, if the circuit had been unknown and $S_I(f)$ were measured, the power spectrum would be of Lorentzian form $F_{RL}(f)$, indicating that the frequency behavior is analogous to a series RL circuit. The corner frequency f_c gives the ratio L/R directly. The circuit elements are therefore identified and determined, to within a scale factor, from the form function $F_{RL}(f)$. If more is known about the system, such as its dc resistance, then the specific R and L values are determined.

The situation is not much more complicated if a capacitance is added to the RL to give a series RLC circuit. Then,

$$|Y|^2_{RLC} = 4\pi^2 C^2 F_{RLC}(f) \tag{2.3}$$

where

$$F_{RLC}(f) = f^2[1 + (Q^{-2} - 2)(f/f_0)^2 + (f/f_0)^4]^{-1} \tag{2.3a}$$

and

$$f_\alpha = (2\pi L/R)^{-1}, \quad f_0 = [2\pi(LC)^{\frac{1}{2}}]^{-1}, \quad Q = f_0/f_\alpha$$

then

$$S_I(f)/S_0 = F_{RLC}(f) \tag{2.4}$$

and

$$S_0 = 4\pi^2 C^2 S_{e_0}. \tag{2.5}$$

The form function $F_{RLC}(f)$ is a resonance with resonant frequency f_0 and shape factor f_0/f_α. Furthermore, it is not necessary to consider a branch with more than two reactive elements since a more complicated admittance can be decomposed by partial fraction expansion.

Consider the circuit of parallel branches shown in Fig. 2*a* and the conditions assumed previously. The total current I is given by

$$I = I_1 + I_2 \ldots I_n$$

where

$$I_i = e_i Y_i \qquad i = 1, n.$$

The power spectrum is then

$$S_I(f) = S_{e_1}|Y_1|^2 + \cdots S_{e_n}|Y_n|^2. \tag{2.6}$$

A measured $S_I(f)$ gives a form function which presumably has one or more features in a given frequency range. Each feature can be dealt with separately provided that each is associated with an ion conduction process. Specific branches may then be assumed and evaluated as to whether they can produce the necessary form function. A reasonable fit of $F(f)$ then gives element values provided that some other information is available. In the particular procedure used here, the ℓHH description and values of the ion conduction admittance gave the initial circuit and element values from which modifications were made and tried. The values of the circuit elements which gave a reasonable fit of the form function for the measured $S_{I_K}(f)$ were used with the addition of a parallel (membrane) capacitance, C_m, element (Fig. 2*b*) to compute the $|Z|$ and ϕ functions of frequency to compare with measurements of these functions.

The form function S_{I_K}/S_0 shown in Fig. 3*a* (filled circles) was taken from data presented by Fishman, Moore and Poussart (1975, Fig. 8, 0mV). In particular, the spectrum defined by the filled circles is the difference between a power density spectrum of current noise before and after substantial reduction of K^+ current flow and normalized by S_0 to compare form. The noise which produced the difference spectrum is K^+ conduction noise since Na^+ conduction noise was at least an order of magnitude lower and may be evident only under special conditions. Thus, in the circuit description shown in Fig. 3*a*, only potassium and leakage conduction are considered. The *RL* and parallel *R* branch are the ℓHH circuit description of potassium and leakage conduction (see Fig. 1*c* with $\bar{g}_{Na}=0$) with element values approximately those obtained using the standard *HH* values at rest potential. The function $|Y_1|^2+|Y_2|^2$ obtained from these two parallel branches alone (each in series with an assumed uncorrelated, excess white-noise source), shown as the dashed curve in Fig. 3*a* does not fit the form of the power spectrum $S_{I_K}(f)/S_0$ in the transition frequency region although the low and high frequency behavior appears to be good. Consequently, another branch of the *RLC* type was added in parallel with the previous two branches as shown in the circuit of Fig. 3*a*. The equation describing the current-noise power spectrum is then

$$S_{I_K}(f)/S_0=|Y_1|^2+|Y_2|^2+|Y_3|^2 \tag{2.7}$$

where $|Y_1|^2$ and $|Y_3|^2$ are given by Eqs. (2.0) and (2.3), respectively, and $|Y_2|^2=R_2^{-2}$. Since the precise characteristics of the equivalent voltage noise sources are presently undetermined, the following assumptions are made on the basis of simplicity and as a framework for description: the sources are assumed to be (1) white, (2) uncorrelated, and (3) equal in intensity. Assumption (3) is a simplification which is justified by the fact that the noise produced in any branch must be comparable to the noise in the other branches in order that its branch elements account for a portion of a particular spectral feature. Eq. (2.7) was programmed for computation with the circuit branches shown in Fig. 3*a*. The computer displayed the functions $|Y_1|^2+|Y_2|^2$, and $|Y_1|^2+|Y_2|^2+|Y_3|^2$ simultaneously on an oscilloscope. $S_{I_K}(f)/S_0$ was also available for comparison with the computed curves. The element values shown in Fig. 3*a* gave an excellent fit (Fig. 3*a*, solid curve) of the form function $S_{I_K}(f)/S_0$.

A 1 μF capacitor was placed in parallel with the circuit (Fig. 3b) with the same element values, determined by fit of the $S_I(f)$ data. $|Z|$ and ϕ functions of frequency were then computed and are shown as the solid curves in Fig. 3*b*. The dashed curves represent the ℓHH type functions

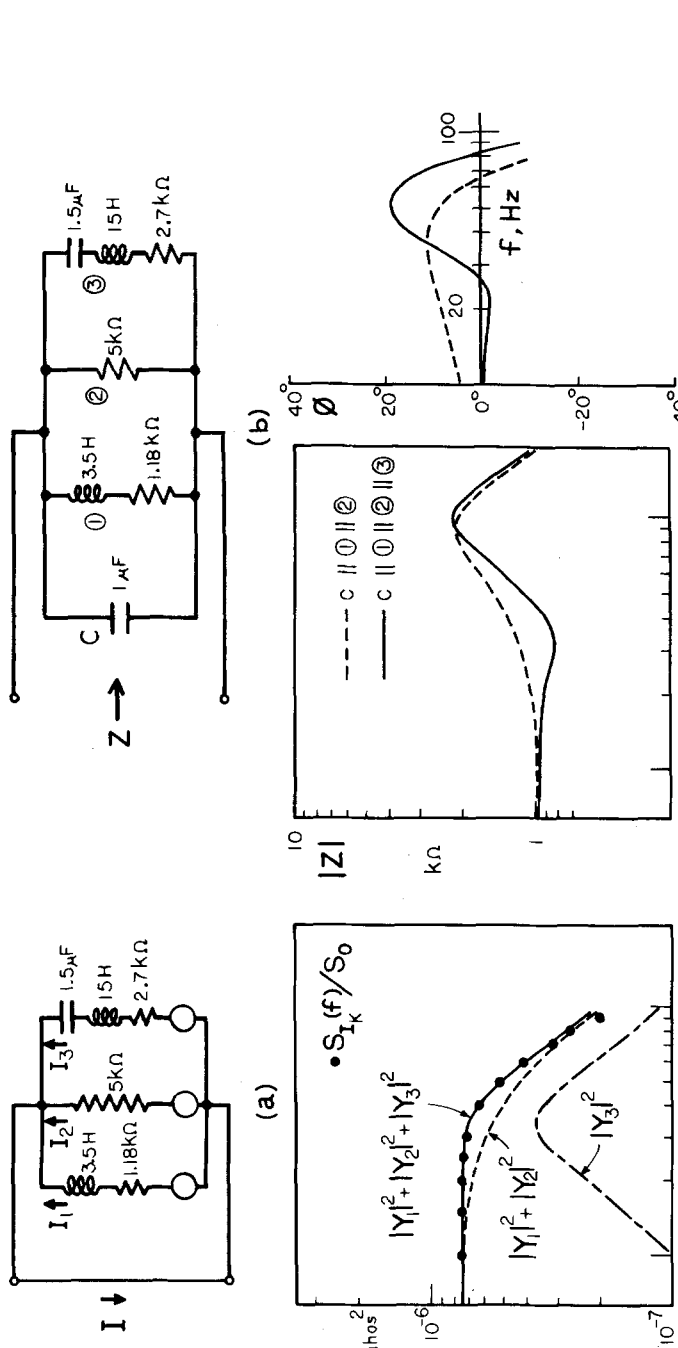

Fig. 3. Implementation of circuit description of K^+ conduction from spontaneous noise data (under constant voltage condition) by modification of circuit from *ℓHH* equations for K^+ and leakage conduction [branches 1 and 2 in (*a*)] to include an additional *RLC* branch (3). The voltage noise sources (open circles in circuit (*a*) are assumed to be white, uncorrelated, and of qual intensity (in excess of thermal noise). The form of the power spectrum is then the sum of the magnitude squared of each branch admittance. The element values were chosen to give a fit (solid curve) of the form function S_{I_K}/S_0 (filled circles), which is the difference between current noise spectra, before and after reduction of K^+ current, measured in an axon patch by Fishman, Moore and Poussart (1975, Fig. 8, 0mV spectra). (*b*) computed |Z| and ϕ functions for circuit and element values determined in (*a*) with additional 1 μF capacitor in parallel. Dashed curves are *ℓHH* type (*C* branch in parallel with branches 1 and 2); solid curves are for the entire circuit, which is based on noise data. The noise data indicate that a low frequency feature consisting of a local minimum in |Z| and negative ϕ should be measurable due to resonance of the additional *RLC* branch in the circuit

for a membrane without Na^+ conduction. A comparison indicates that the sharp corner in noise spectra should produce a K^+ conduction related low frequency feature in membrane impedance which is not contained in the ℓHH description. Specifically, a local minimum ("dip") occurs in $|Z|$ at about 35 Hz and ϕ is negative at low frequencies instead of being positive. These predictions could then be checked by employing the measurement techniques described subsequently.

Materials and Methods

Preparation

Axons from the squid *Loligo pealei*, which were received live at the Marine Biological Laboratory, Woods Hole, Massachusetts, were used in these experiments. The procedure for obtaining an experimental preparation from animals was the same as described previously (Fishman, Poussart & Moore, 1975).

Chamber

The chamber was described previously (Fishman, 1970; Fishman, Poussart & Moore, 1975). The solution flow into and out of the chamber, however, was matched by adjustment of a needle valve. This system produced a smooth flow and nearly constant solution volume, which prevented low frequency noise due to fluctuations in conduction between the axon and external ground electrode.

Solutions

Natural sea water (*SW*) was used as the external solution. For internal perfusion experiments, the standard perfusate was 0.5 M KF and 5 mM Tris × HCl, pH 7.5 at 22 °C. A low-potassium perfusate consisted of 50 mM KF, 50 mM CsF, 5 mM Tris × HCl and 0.64 M sucrose. The method of internal perfusion was as previously described (Fishman, 1970).

Axial Wire

The electrodes and experimental scheme are shown in Fig. 4. A "piggyback" electrode (Fishman, 1970) consisting of a platinized platinum (Pt – Pt) axial wire mounted atop a potential pipette (Fishman, 1973) constituted the internal electrodes. The axial wire extended from the entry point, where it was insulated with wax, through the entire axon in the chamber and into the air gap at the other end of the axon (Fig. 4). The air gaps isolated the portion of axon in the chamber from the cut ends over the posts. An external reference pipette was used to record the potential differentially with respect to the internal pipette. A 1.5 cm length of Pt – Pt wire (0.032″ diameter), placed parallel to the axon and 1 mm from it, was held at virtual ground by an operational amplifier which was used to record transmembrane current.

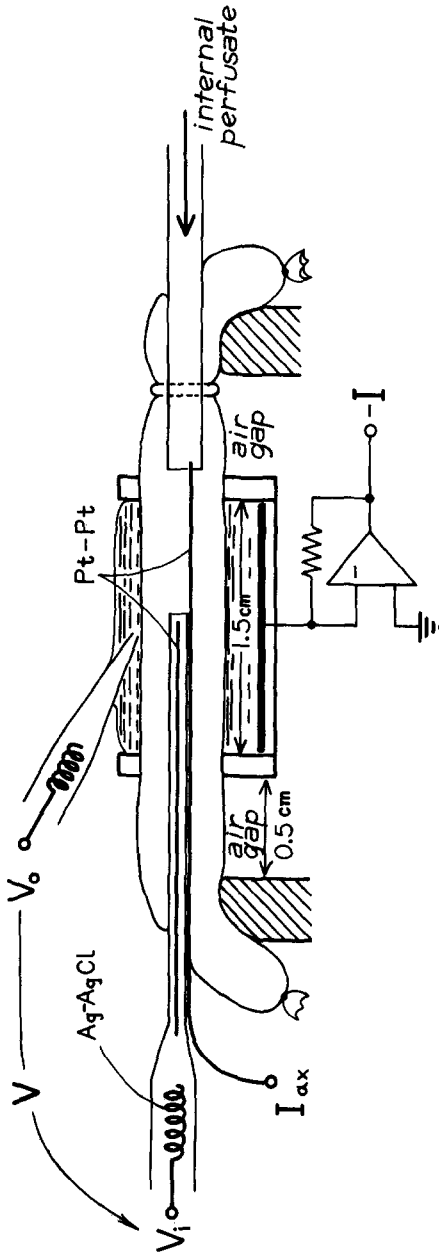

Fig. 4. Diagram of axial wire measurement. *See* text for details

In an attempt to minimize current electrode and axon end effect distortion, guarded impedance measurements were made. The internal piggyback electrode was modified to include two axial (75 μ diameter) platinum wires mounted colinearly on the top and bottom surfaces of the potential pipette. Wire 1 was insulated except for a platinized 5 mm length, which was centered at the aperture of the potential pipette. Wire 2 was insulated in the central 5 mm length and contained two 5 mm platinized lengths on both sides of the insulated central

length. Wire 1 was connected directly to the current source output and wire 2 was driven from a voltage follower which was connected to the current source output. This measurement scheme was abandoned, however, because electrode polarization effects in wires 1 and 2 could not be matched. Consequently, the guard signal produced a frequency dependent distortion which affected the impedance measurement in the central region. We judged the aberration to be more severe than the distortion produced without guards in large area measurements. The details and analysis of this guarded measurement are left to a future technical note. Furthermore, guard schemes produce high extraneous noise conditions in the measurement of membrane current as a consequence of the low resistance between guards and central electrode (Fishman, Poussart & Moore, 1975).

Impedance and Admittance Measurements

Fig. 5 shows the measurement and data processing instrumentation. Two signal sources were used in these experiments. White noise (Hewlett-Packard model 3722A), which had a Gaussian amplitude distribution and could be band-width limited between 50 Hz and 5 kHz, to prevent aliasing in subsequent analysis instrumentation, was applied to the axon. Sinusoids were applied with an Interstate Electronics Corp. model F 34 either at discrete frequencies or in a logarithmic sweep mode from 1–30 Hz. To measure impedance (Z) the source signal was applied to the axon as a constant current (CC) and the transmembrane potential response (V) and membrane current (I, Fig. 4) were recorded on two channels of an FM tape recorder (Hewlett-Packard model 3960A). To measure admittance (Y) the source signal was applied as the command to a voltage clamp system (Fishman, 1970). In this case, the membrane current response (I) and transmembrane potential (V) were recorded on tape.

The noise data were processed in two ways. The magnitude of Z and Y *vs.* frequency was obtained by analysis of the response (either V or I) with a real-time spectrum analyzer (Honeywell model 52). In addition, the stimulus and response were cross-correlated ($X\ COR$) and Fourier transformed (FTA) using a Honeywell model 43A and 470A to obtain both magnitude and phase functions of frequency. The spectrum analyzer contained filters to prevent aliasing (*see* Bendat & Piersol, 1971); however, the correlator did not. Thus, a pair of operational filters (Rockland model 1000F) were matched to within 2° for phase *vs.* frequency characteristics, and used in conjunction with the correlator whenever analysis was done for band-widths below that of the applied noise. The sinusoidal data processing was done by direct $X-Y$ plots on a recorder after a $16\times$ reduction of the tape speed during playback. The reduction lowered the uppermost frequency from 30 to less than 2 Hz which could then be plotted directly. The swept-frequency sinusoidal data were processed by a Hewlett-Packard model 3575A gain/phase test set.

During an experiment, the magnitude of Z and Y was monitored in a particular frequency band with the spectrum analyzer. The phase function was observed for sinusoidal inputs as a Lissajous (ellipse) pattern on an XY oscilloscope. This procedure allowed a relatively fast assessment of the impedance and admittance properties of an axon. Then spectral analysis was used to monitor the data which was being recorded for noise inputs, and Lissajous figures were monitored during application and recording of sinusoidal stimuli. Extensive processing of the data was done, subsequent to experiments, from the analog tape recordings.

Calibration

As a check of the data processing instrumentation, the phase ϕ and magnitude of impedance $|Z|$ of a linear, lumped electrical circuit (inset, Fig. 6) were measured. The circuit configuration chosen corresponds to the admittance obtained from the linearized Hodgkin-

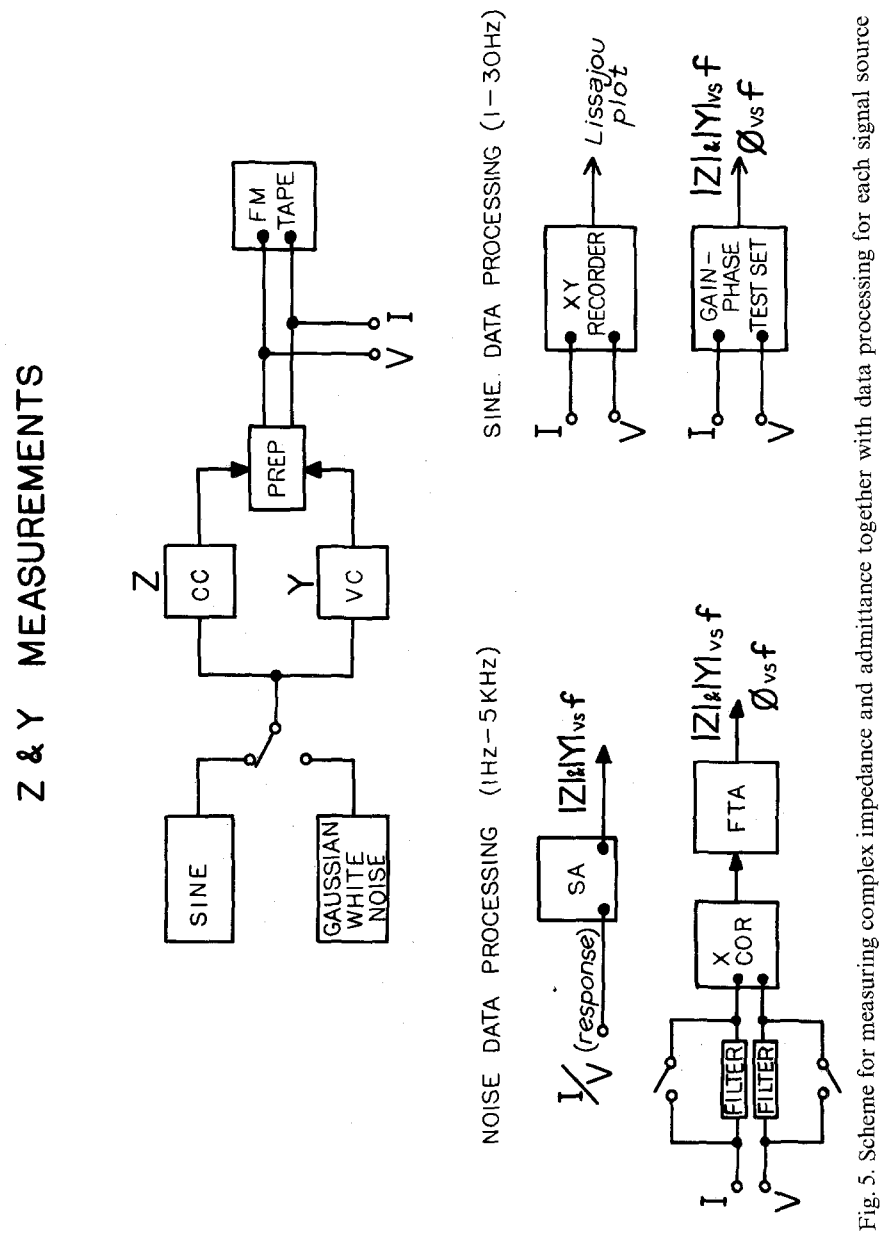

Fig. 5. Scheme for measuring complex impedance and admittance together with data processing for each signal source used

Huxley equations when membrane capacitance, K^+ conduction and leakage are considered in the absence of Na^+ conduction (*see* Fig. 1*c* with $\bar{g}_{Na}=0$). The circuit element values were selected for convenience and as an approximation to the *HH* values at rest potential. The element values were measured with a bridge so that computation of $|Z|$ and ϕ *vs.* frequency (solid curves, Fig. 6) could be compared with measurements. The $|Z|$, measured by spectral analysis of the response to an applied white noise current, is shown in the upper portion of the figure. The noise estimate of the magnitude has been redrawn from three separate analysis bands 0.125–50 Hz, 0.5–200 Hz, and 12.5 Hz–5 kHz, for which 128 spectra have been averaged

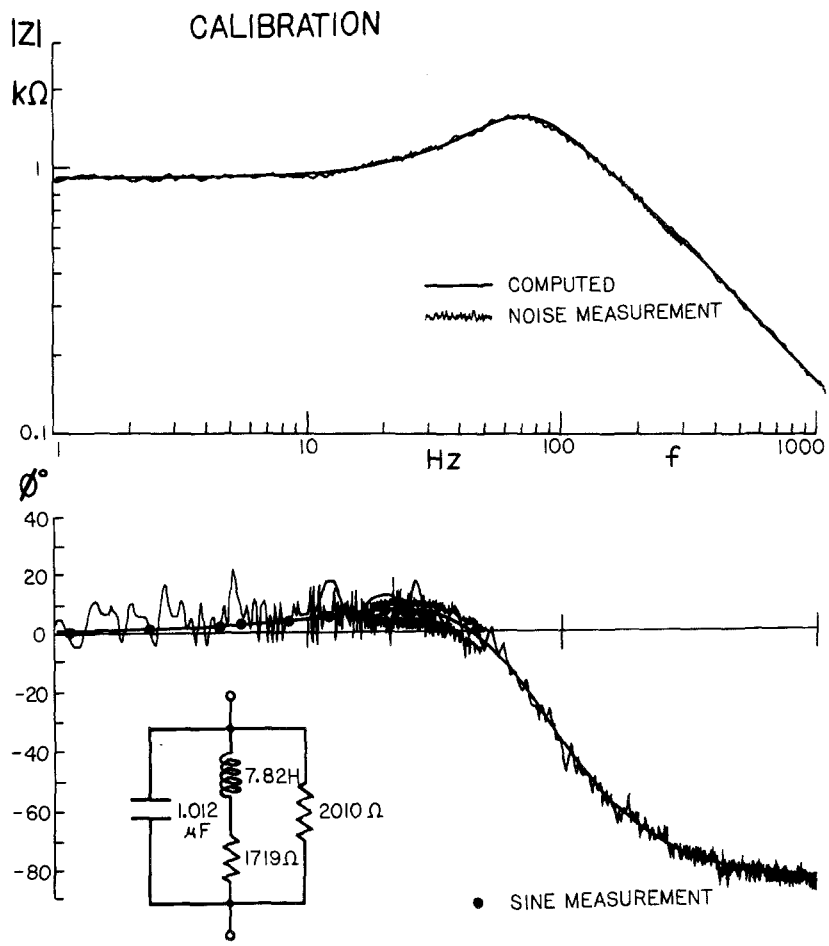

Fig. 6. Calibration of data processing instrumentation by comparison of measured $|Z|$ and ϕ functions with computations for the lumped electrical circuit shown, which is the ℓHH type (*see* Fig. 1*c*, $\bar{g}_{Na}=0$)

with a data length of 1024, 256, and 102 sec in each respective band. In the lower portion of Fig. 6 the phase function was produced by the correlator-Fourier transformer combination from noise measurements in two bands, 50 Hz and 1 kHz. The same data length of 30 sec was analyzed in each band and consequently the lower band analysis yields phase estimates with greater variance. Nevertheless, smooth curves drawn through the estimate yield accuracy to within 3° over the entire frequency range. In addition, the sinusoidal measurement of phase in the range 1–30 Hz produced accuracy to within 1°. The maximum peak to peak experimental perturbation of membrane potential produced by noise or sinusoidal sources was 3 mV. Nearly all of the sinusoidal data were obtained at the 3 mV level in order to produce a maximum signal-to-background noise ratio (40 db) which gave experimental accuracy within 1° in the phase measurements. There was insignificant degradation in the noise estimates of phase with perturbation level since the noise method involves cross-correlation of

stimulus with response, which is inherently insensitive to extraneous noise (Fig. 10, Fishman, 1975). The experimental noise and sinusoidal phase data presented were all checked to assure agreement (*compare* Figs. 10 and 11).

Conventions

Membrane potentials in this paper are absolute transmembrane potentials without correction for liquid junction potentials. Changes in rest (R) potential are positive for depolarizations and negative for hyperpolarizations. Membrane areas were computed on the basis of the average between the largest and smallest diameter of the portion of a fiber in the measurement chamber. Since the axons were usually nonuniform in diameter, it is likely that the area estimates are in error by at least 20%. The impedance and admittance scales of data presented are thus in ohms or mhos with an estimated area (corresponding to each axon) listed in each caption. However, the impedance computations from the *HH* equations are in ohm $\times$ cm^2.

Results

Linearity

To determine whether the perturbing signals which were applied to the membrane resulted in linear responses, two types of measurements were made. First, the magnitude and phase of membrane response V_m were evaluated for applied noise currents which produced membrane potential perturbations ranging from spontaneous noise (50 μV peak-to-peak) up to 10 mV peak-to-peak (Fishman, 1975). The impedance function obtained was invariant for this range of membrane potential displacements. The noise measurement of complex impedance was therefore adequate even at the level of spontaneous fluctuations where the applied noise was of the same intensity as the background.

As a second check of linearity, impedance and admittance functions were measured in the same axon. This comparison, shown at rest potential in Fig. 7, indicates that the impedance and admittance functions are, within the limitations of the two measurements, reciprocals of one another. The measurement of a proportionate response to increases in stimulus as well as verification of the reciprocal nature of impedance and admittance are strong indications of linearity for perturbations below 10 mV peak-to-peak. However, these tests were not expected to provide quantitative information on the degree of linearity. An appropriate method for evaluation of the degree of nonlinearity would be to apply the Wiener theory of nonlinear system identification as described by Marmarelis and Naka (1974).

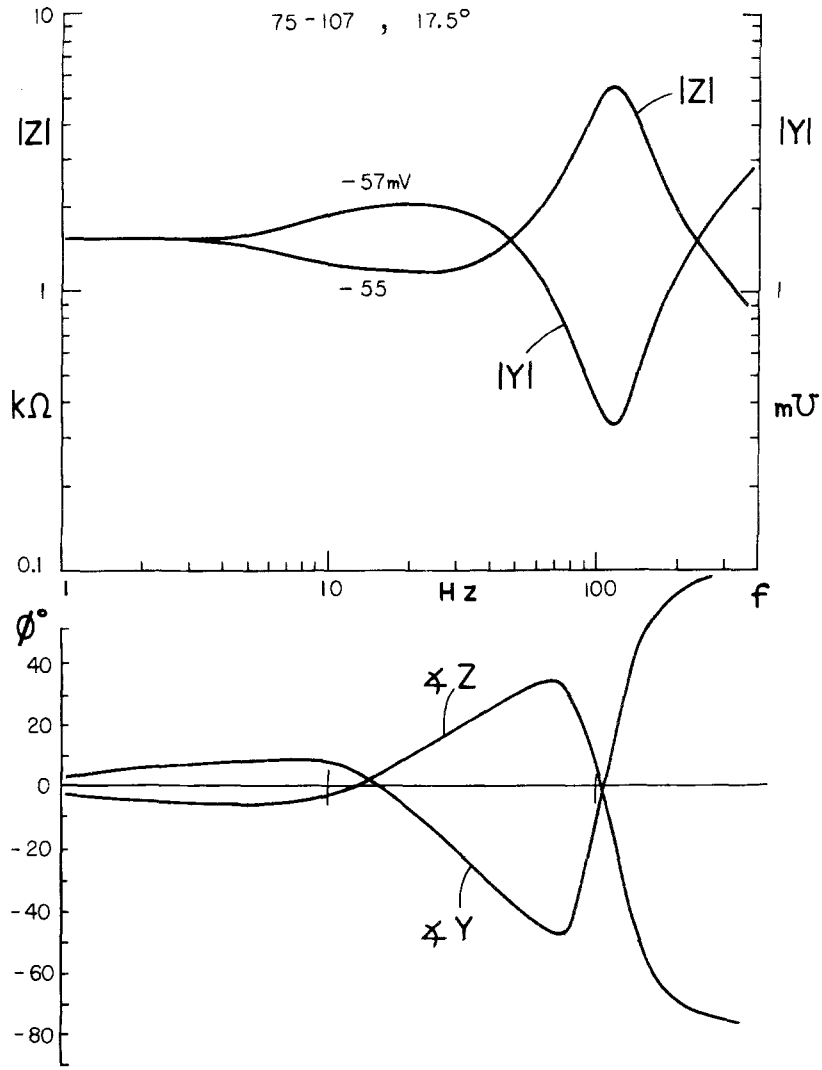

Fig. 7. Magnitude and phase functions of the impedance (measured during constant current) and admittance (measured during voltage clamp) of squid axon membrane near rest potential. Z and Y are nearly mirror images of each other, which is indicative of a reciprocal relationship and linearity. The low frequency (1–30 Hz) behavior is not accounted for in the ℓHH description of membrane conduction (*see* Fig. 3*b*). Membrane area approximately 0.2 cm^2

Impedance and Admittance

The most prominent aspect in the $|Z|$ and $|Y|$ in Fig. 7 is the resonance and anti-resonance at 120 Hz and the accompanying phase associated with the resonance. The linearized HH equations account for the resonance (*see* Fig. 14) as a consequence of the frequency dependent properties of

K^+ and Na^+ conduction which produce *RL* branches in parallel with membrane capacitance (Fig. 1*a*). The low frequency (1–30 Hz) behavior, however, is not contained in the linearized *HH* equations. Specifically, the negative phase and dip in $|Z|$ at low frequency are not found in the *HH* circuit description of conduction (see Fig. 3*b*). This low frequency feature also occurs in the admittance, which can be seen in Fig. 7 as the mirror image of the impedance.

The measurement of a local minimum in the $|Z|$ at low frequencies is not, by itself, definite evidence of an axon related feature. However, the negative phase accompanying the minimum in $|Z|$ strongly indicates that the measured impedance behavior correlates with the driving function and is not due to extraneous artifacts. Impedance measurements of the electrodes in *SW* with the chamber current-electrode in series with a 3.3 kΩ (equivalent axon source resistance) to ground gave a flat magnitude and zero phase function from 1 Hz to 1 kHz. In addition, after several axon experiments, which gave the low frequency feature, the axon's functional characteristics (rest potential, leakage, etc.) were degraded by exposure externally to a *SW* solution with pH 2 with the electrodes and all other measurement conditions the same. Under these conditions, the feature disappeared. Furthermore, it was established unequivocally by sinusoidal phase (Lissajous pattern) measurements (accuracy to within 1°) that in normal axons the phase function was zero at three points along the frequency axis. The frequencies of zero phase were apparently dependent on numerous factors, but generally they occurred in distinct ranges: 1 to 3 Hz, 8 to 20 Hz, and 60–150 Hz.

Impedance Variation with Potential

The variation of impedance and admittance was measured during applied dc currents and potentials which produced membrane potential excursions of ±15 mV about the rest potential. The range was restricted to these relatively small potential excursions because axon deterioration was evident following excursions beyond these limits. This observation is curious since it is possible to polarize squid axon to potentials of 30 mV or more from rest without significant damage in small area measurements (Fishman *et al.*, 1975), and it is also possible to substantially polarize nodal preparations from rest for prolonged periods (Siebenga, Meyer & Verveen, 1973). Axon deterioration for large continuous polarizations

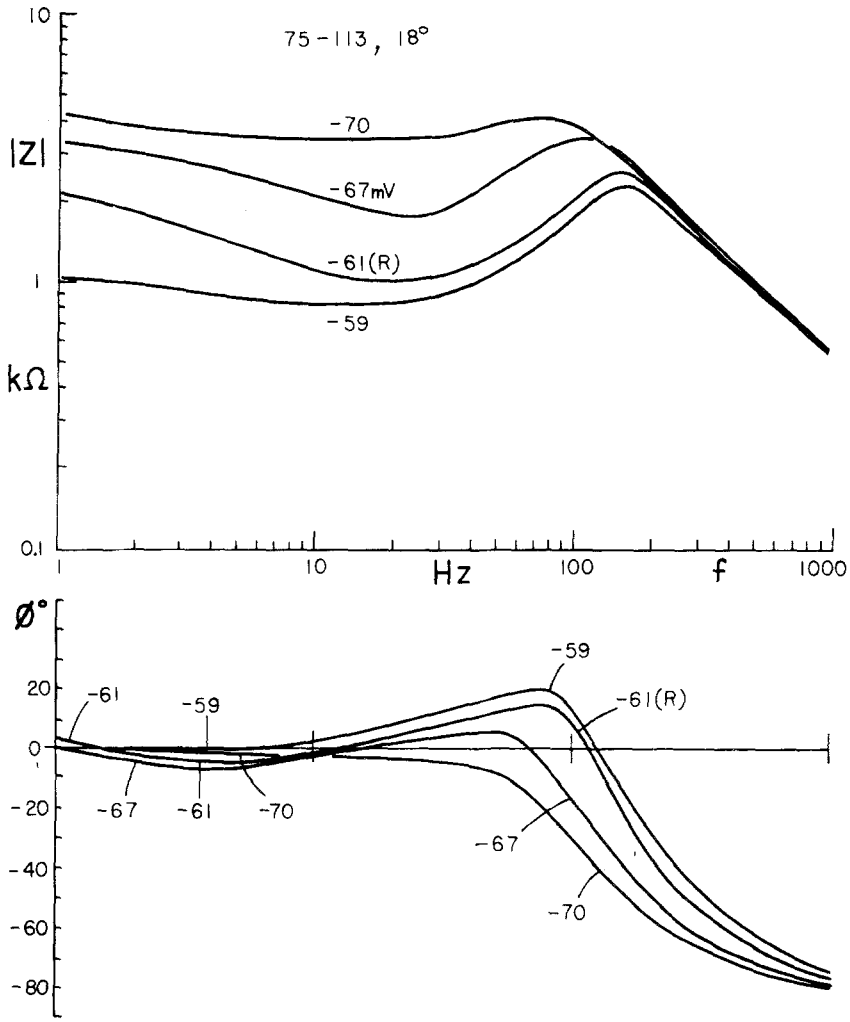

Fig. 8. (*a*) Magnitude and phase of membrane impedance for polarizations to the indicated potentials by passage of constant current through the membrane. Note that the "dip" in $|Z|$ is diminished for depolarization (−59 mV) from rest (*R*), but is enhanced for small hyperpolarization (−67) and again diminished upon further hyperpolarization (−70). ϕ is zero at three frequencies as membrane potential changes from depolarized to hyperpolarized values and at −70 mV does not cross the frequency axis because the parallel resonance (peaking in $|Z|$) is also diminished. Membrane area approximately 0.2 cm^2

during axial-wire measurements may be due to internal pH changes produced at the Pt − Pt current wire. However, these effects also occurred during internal perfusion with buffered perfusate. Nevertheless, it appears that there is some degradation associated with long duration currents applied through a Pt-Pt wire within axons.

Fig. 8 shows $|Z|$ and ϕ functions measured over the frequency range 1-1000 Hz with white noise applied as a current and superposed on a dc current to produce the steady-state membrane potentials indicated. The usual resonance, apparent at rest (R), becomes less pronounced with hyperpolarization as the potassium equilibrium potential is approached. This behavior is expected from the *HH* description (Mauro *et al.*, 1970). The low frequency (dip and negative phase) feature, however, becomes more pronounced with a slight hyperpolarization (-67 mV curves) which produces a maximum negative phase of 10° at 3.5 Hz. Further hyperpolarization to -70 mV diminished both dip and negative phase. In contrast, depolarization (-59 mV) diminished the dip and produced nearly zero phase at frequencies from 1-5 Hz. This behavior with potential was observed in all axons, although particular aspects such as the potential for maximum negative phase varied. For example, in some axons low frequency negative phase was not present at rest or depolarized potentials, whereas for increasing hyperpolarization it was present, reached a maximum, and then diminished. In addition, the phase function at frequencies between 1 and 2 Hz sometimes crossed zero and became positive as seen in Fig. 8 (-61 mV, ϕ function) and Figs. 10 and 11 (-59 and -56 mV, ϕ functions). The zero phase crossings of the frequency axis as well as the phase polarity could be determined quite accurately ($<1\%$) from the collapse of oscilloscope ellipses, which were generated by simultaneous display of a single-frequency sinusoidal stimulus as a function of the response, and the observation of the direction of rotation of the elliptical trace with changes in frequency. The voltage behavior of the low frequency impedance feature is an important consideration with respect to phenomenological interpretations (*see* Discussion).

Temperature Effects

Most measurements were made at temperatures between 12 and 19°C which produced resonances at 100 Hz or more and allowed characterization of the low frequency feature between 1 and 30 Hz. At low temperatures, this feature shifts to lower frequencies and becomes more difficult to measure. Fig. 9 shows impedance functions measured in the same axon at two temperatures. Both the resonance and low frequency feature shift to lower frequencies with a decrease in temperature.

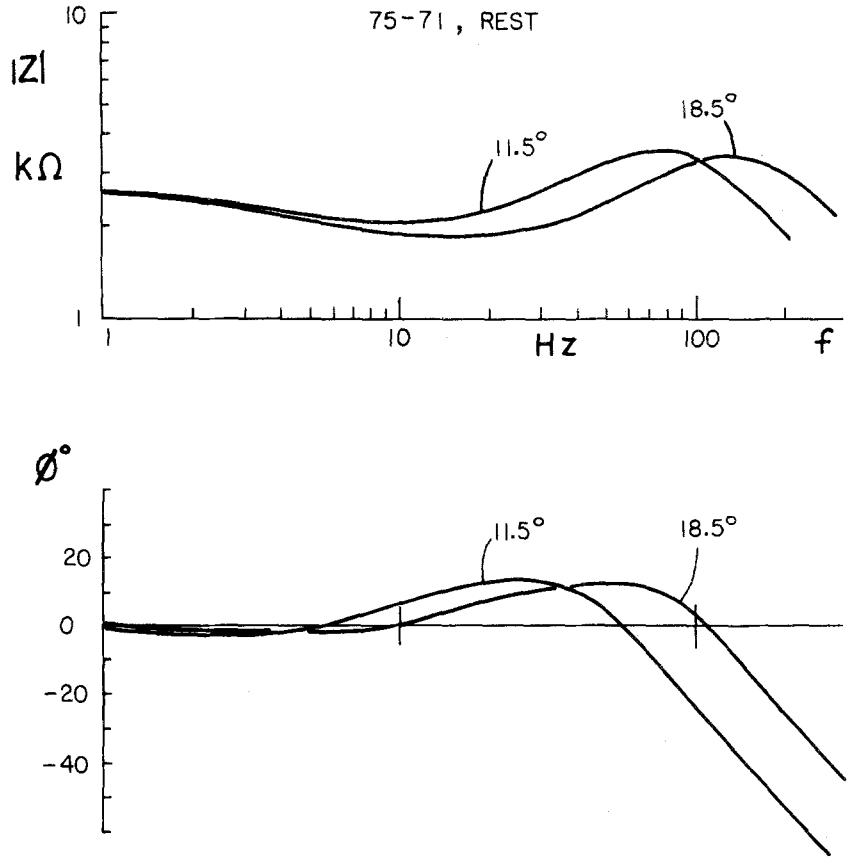

Fig. 9. Effect of temperature change on low frequency impedance at rest potential. Membrane area approximately 0.17 cm^2

Tetrodotoxin (TTX)

The application of TTX, externally, alters the impedance resonance, making it much broader, but TTX does not eliminate it. It is apparent that while Na^+ conduction does enter into the impedance resonance at potentials around rest, K^+ conduction in conjunction with membrane capacitance accounts for a substantial portion of the impedance resonance. Fig. 10 shows data from an axon after exposure to TTX. The low-frequency dip and negative phase persist after blockage of Na^+ conduction as does the impedance resonance. Fig. 11 contains phase functions taken from the same axon as the data in Fig. 10, but for sinusoidal stimuli which were applied during a logarithmic sweep of frequency from 1–30 Hz. The negative phase property is apparent again in the presence of TTX, and these phase data corroborate the corresponding phase functions in Fig. 10, which were produced by the noise method.

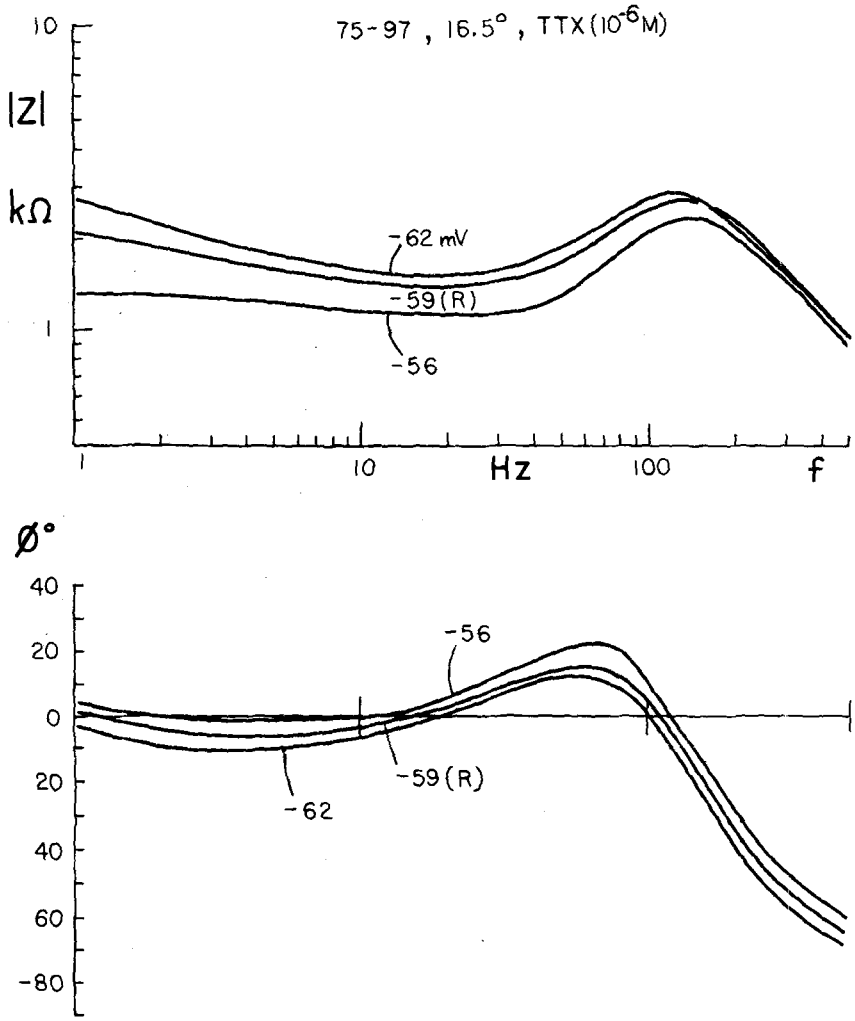

Fig. 10. Magnitude and phase of membrane impedance after block of Na^+ conduction with tetrodotoxin added to the external solution. The resonance between 100 and 200 Hz arises from the interaction of K^+ conduction inductive reactance and membrane capacitance (Fig. 1*c*, $\tilde{g}_{Na}=0$). The low frequency feature occurs despite Na^+ conduction block. Note the third zero ϕ crossing of frequency axis between 1 and 2 Hz at rest and depolarized potential. Membrane area approximately 0.18 cm^2

K^+ Conduction Dependence

In order to observe the dependence of impedance and admittance on K^+ conduction two types of measurements were made. First, Na^+ conduction was blocked with TTX externally and the impedance with and

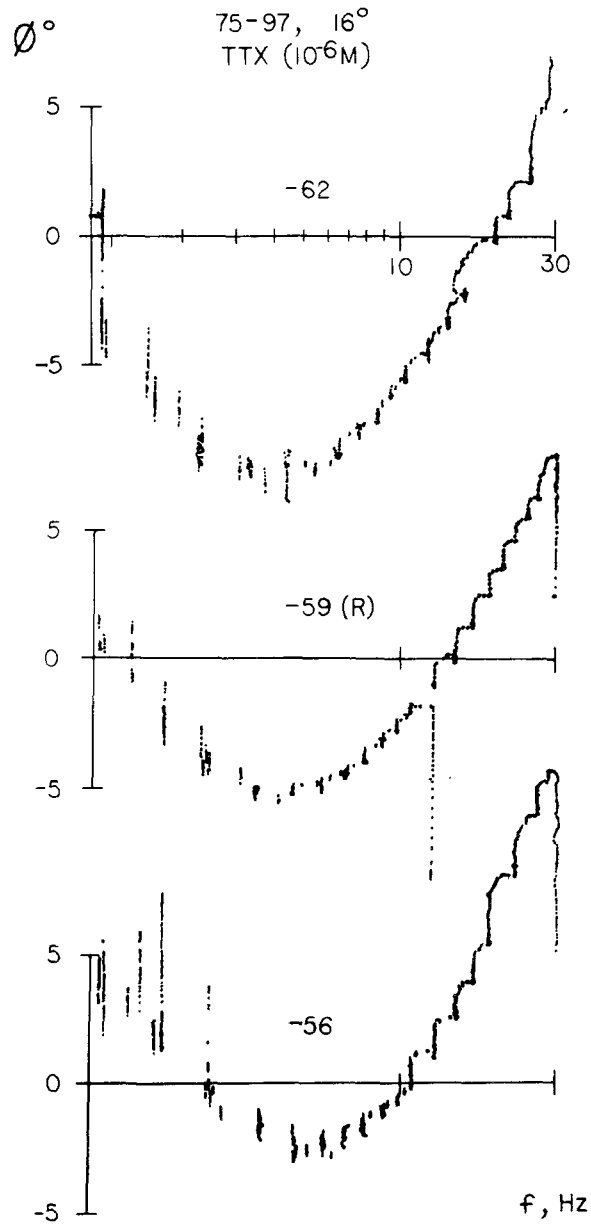

Fig. 11. Low frequency phase of membrane impedance produced by logarithmic changes of frequency of sinusoids applied to the membrane. Conditions and axon are the same as those measured by applied noise techniques in Fig. 10. The phase data for the two different sources are in agreement

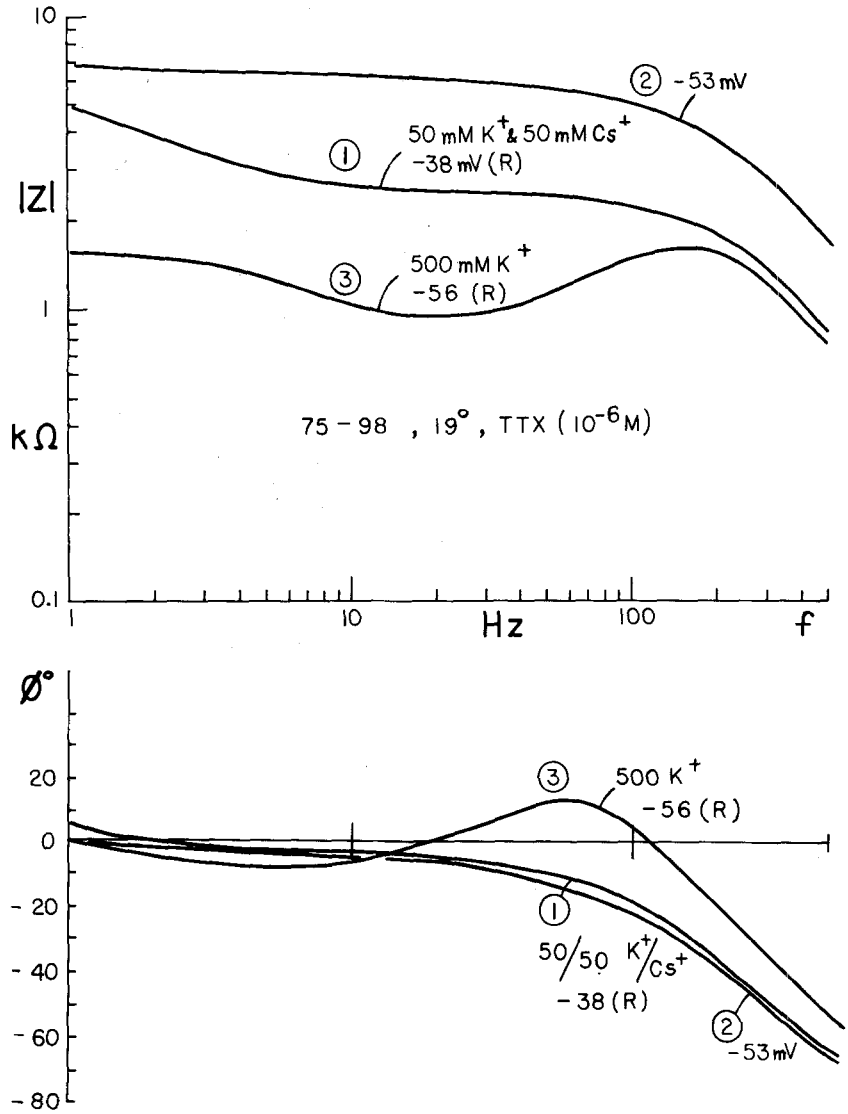

Fig. 12. Effect of substantial reduction in K^+ conduction, during block of Na^+ conduction, on magnitude and phase of membrane impedance. With TTX in the external solution, sequence is (1) internal perfusion with low K(F) and Cs(F) perfusate; no resonance or low frequency feature is present; however, axon rest potential is depolarized (−38 mV) from normal rest. (2) Polarization of axon to −53 mV does not change form of impedance; thus potential does not account for absence of resonance or low frequency feature. (3) Internal perfusate changed to 500 mM KF + buffer; K^+ resonance and low frequency feature reappear with restoration of K^+ conduction and active transport is excluded by virtue of presence of fluoride in perfusate. Axon area approximately 0.18 cm^2

without K^+ conduction was compared. Fig. 12 shows these data. In the presence of TTX, the axon was first internally perfused with a low concentration KF perfusate containing CsF in addition. The axon impedance, under these conditions, is essentially that of a parallel *RC* circuit with a flat magnitude (except at very low frequency) which rolls smoothly into a high frequency decline. The phase function also has an appearance which is characteristic of an *RC* circuit showing only increasing negative phase with increasing frequency. This behavior is expected since the voltage-dependent ion conductances are insignificant compared to leakage. Perfusion with the low $[K_i^+]$ perfusate gave a rest potential (-38 mV) which was less than that in the presence of normal $[K_i^+]$ perfusates. Thus the potential was polarized to -53 mV and intermediate potentials without any indication of the low frequency feature previously described. Finally, the perfusate was changed from the low *KF* to the standard (normal *KF*) solution and, as seen in Fig. 12, both the resonance and low frequency feature appeared in $|Z|$ and ϕ. The presence of the low frequency feature during perfusion with 0.5 M KF(1) eliminates active transport as a possible source of this phenomenon since internal perfusion with fluoride stops "pump" activity (Brinley & Mullins, 1967; Canessa-Fischer, Zambrano & Rojas, 1968) and (2) suggests that the low frequency impedance is associated with the K^+ conduction process.

In the second type of experiment, the admittance was measured in the presence of Na^+ conduction without significant K^+ conduction. These data are shown in Fig. 13. The axon was again internally perfused with the low $[K_i^+]$ solution (50 mM KF + 50 mM CsF + buffer) to drastically reduce K^+ conduction. The solid curves in Fig. 13 are the measured admittances (during voltage clamp) for the indicated clamp holding potentials with *SW* externally. A new anti-resonance appears under these conditions which is distinguished from the anti-resonance which occurs with K^+ conduction intact in that (1) it occurs at much lower frequencies (*compare* Fig. 13 with *Y* in Fig. 7) and (2) it is eliminated after TTX is added to the external *SW* (dashed curve, Fig. 13). The new resonance which occurred in both impedance and admittance measurements thus appears to be associated with interaction between the Na^+ conduction process and membrane capacitance. This resonance reflects the interaction of the inductive reactance associated with the *h* process of the Na^+ system with the other capacitive reactances, as can be seen in Fig. 1*b* with the contribution of the K^+ system substantially reduced. It is reasonable to expect that this condition, in which the Na^+ system dominates the total membrane behavior, would be very favorable for the observation

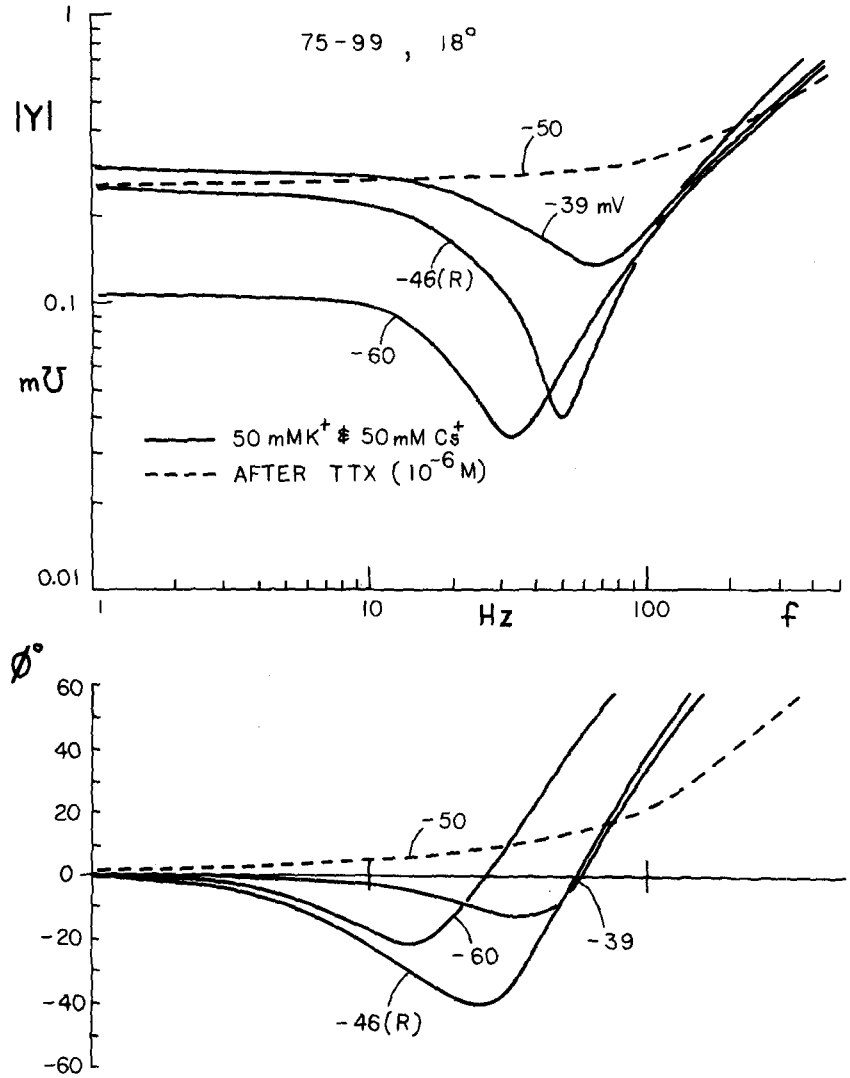

Fig. 13. Effect of substantial reduction in K^+ conduction, before and after block of Na^+ conduction, on magnitude and phase of membrane admittance. Admittance with potential change about rest during internal perfusion with low K(F) and Cs(F) perfusate. The anti-resonance is due to Na^+ conduction interaction with membrane capacitance since the resonance (1) occurs at lower frequencies than K^+ resonance (*compare* Fig. 10), (2) occurs in spite of substantially reduced K^+ conduction (*compare* Fig. 12, curves 1 and 2), and (3) disappears after Na^+ conduction is blocked by TTX added externally (dashed curves). Note low frequency feature in admittance (*compare* Fig. 7, *Y*) is absent in these data regardless of the state of Na^+ conduction

of spontaneous Na^+ conduction noise. However, noise measurements under these circumstances have indicated that the intensity of Na^+ conduction noise is so small as to be marginally observable (Fishman, Moore & Poussart, 1975). Further details concerning the sodium system resonance will not be considered in this communication. The significant result with respect to the present work is that the low frequency feature is absent (*compare* Fig. 13 with Y data in Fig. 7). Thus a low-frequency mode is measured only when K^+ conduction is normal and without any apparent dependence on the state of Na^+ conduction.

Discussion

Spontaneous conduction noise data are a direct measure of the statistical (microscopic) phenomena associated with ion conduction. These data provide information which can be used to compare kinetic models (Fishman, 1973*a*; Fishman, 1975; Fishman, Moore & Poussart, 1975). To assure that our noise data are characteristic of membrane conduction processes, it seemed desirable to use an alternative means of describing ion conduction at the macroscopic level, which could confirm the noise measurements. Complex impedance and admittance measurements at low frequencies are considered to be the best available counterpart to fluctuation measurements because they are steady-state measurements at small signal levels which give a linearized description of conduction.

The ℓHH equations were used as a model of ion conduction to give a circuit description which could be compared with (1) computations of complex impedance based upon noise data and (2) actual measurements of complex impedance. Complex impedance and admittance data are consistent with computations based upon K^+ noise data (Fishman, Moore & Poussart, 1975) and are, therefore, a strong indication of the validity of the noise data. Both noise and impedance data, however, show important features which are not contained in the ℓHH description of K^+ conduction as well as significant differences in some conduction parameters of *Loligo pealei* axons. In the subsequent discussion, we consider the latter point first since conduction parameters are important in comparing computations from the ℓHH model with data. Secondly, we examine the possibility that the HH description of axon membrane is correct and that the measured discrepancy can be accounted for by extra membrane phenomena.

Adequacy of HH Parameter Values in Describing K^+ Conduction in Loligo pealei

A systematic study of the adequacy of the *HH* parameter values in describing conduction in Woods Hole squid axons has not been reported. The measurements described in this communication were not exhaustive in the statistical sense (number of axons) or in variation of experimental conditions (coverage of membrane potential or temperature). Nevertheless, by visual comparison of the same kind of data from 48 axons, data were selected from one axon, which was representative of several axon experiments at the same temperature. The data shown in Fig. 8 are a typical set of impedance measurements at 18° C. Computations of $|Z|$ and ϕ from the ℓHH equations using the standard *HH* values (Fig. 14*a*) gave an obviously poor quantitative account of the representative axon data (Fig. 8) for the same conditions of temperature and potential changes from rest. This comparison indicates that the ℓHH description does not contain the low frequency feature and that the resonance portion of the curve is not fit well either. The latter discrepancy can be remedied simply by changes in parameter values to give a reasonable fit of the usual resonance portion of the impedance data. However, the low frequency behavior requires an additional process (either a membrane phenomenon such as K^+ inactivation or an extra membrane phenomenon such as K^+ accumulation) not included in the original *HH* equations.

Ignoring the absence of the low frequency feature in the ℓHH computations, there are three apparent discrepancies: (1) The computations (Fig. 14*a*) show no resonance at hyperpolarized potentials of -6 and -9 mV from rest whereas the data (Fig. 8) at these potentials (-67 and -70 mV) show clear evidence of resonance; (2) the height of the resonance (minimum to maximum) in computations at 18° C is reduced at rest potential (and other potentials) from the resonance in real axons; and (3) the resonant frequency and shape of the resonance curve at rest and depolarized potential differ. It is clear that (1) above can only arise from improper K^+ conduction parameters since Na^+ conduction is substantially inactivated at hyperpolarized potentials. (This point was verified in experiments with TTX). The ℓHH computation at 6.3° C gives a significant resonance at rest potential. Thus the Q_{10} [Eq. (1)] was changed from 3 to 2 to reduce discrepancy (2) above. The resonance at hyperpolarized potentials was still not present. Next, $\bar{g}_K$ and V_K were increased from 36 to 50 mmho/cm^2 and from -12 to -22 mV to eliminate disagreement (1) above. The change to the new values of $\bar{g}_K$ and V_K also produced the

proper correction in resonant frequency. Finally, g_L was changed from 0.3 to 0.6 mmho/cm^2 to produce a diminished phase slope above 100 Hz as indicated in the data (Fig. 8). The result of all the above parameter adjustments is shown in Fig. 14*b*, which compares reasonably well with the data of Fig. 8.

The preceding analysis suggests that the Woods Hole squid axon has a substantial K^+ current at rest and hyperpolarized membrane potential by virtue of an increased $\bar{g}_K$ and more negative V_K. The observation of K^+ current noise (Fishman *et al.*, 1975) at hyperpolarized potentials in small patches of axon, isolated with sucrose solution, could be a consequence of this enhanced K^+ current (at rest and more negative potentials) above that in the *HH* description. An implied increase of K^+ current in both spontaneous noise and impedance data again suggests the consistency of the two types of measurements taken with different techniques.

The present results also demonstrate that noise measurements of complex impedance can provide a rapid and accurate linearized description of membrane ion conduction. The speed of acquiring and processing impedance data via this method facilitates the application of impedance measurements to membranes to obtain data under a wide range of experimental conditions. Functional fits of complex impedance data in the frequency domain can be used as the basis for synthesis of circuits which give a detailed description of conduction. The discrepancies between the *ℓHH* description and Woods Hole squid axon data suggest that such data are necessary in order to compare and evaluate models of conduction.

Extra Membrane Phenomena—Diffusion Polarization

Individually and together, the noise and impedance measurements strongly suggest that squid axon K^+ conduction kinetics are not adequately described by a single first order rate process. However, it is possible that the higher order behavior arises not from the conduction kinetics of the axon membrane itself but from phenomena associated with the sheath which surrounds the axon. These effects may be classified as diffusion polarization effects since the ion flows to or from the axon membrane are limited by a diffusion barrier which produces ion depletion or build-up near the membrane.

Frankenhaeuser and Hodgkin (1956) found that the effects of repetitive stimulation and increased $[K_0^+]$ on the action potential undershoot (brief period of hyperpolarization after a spike, called the positive phase)

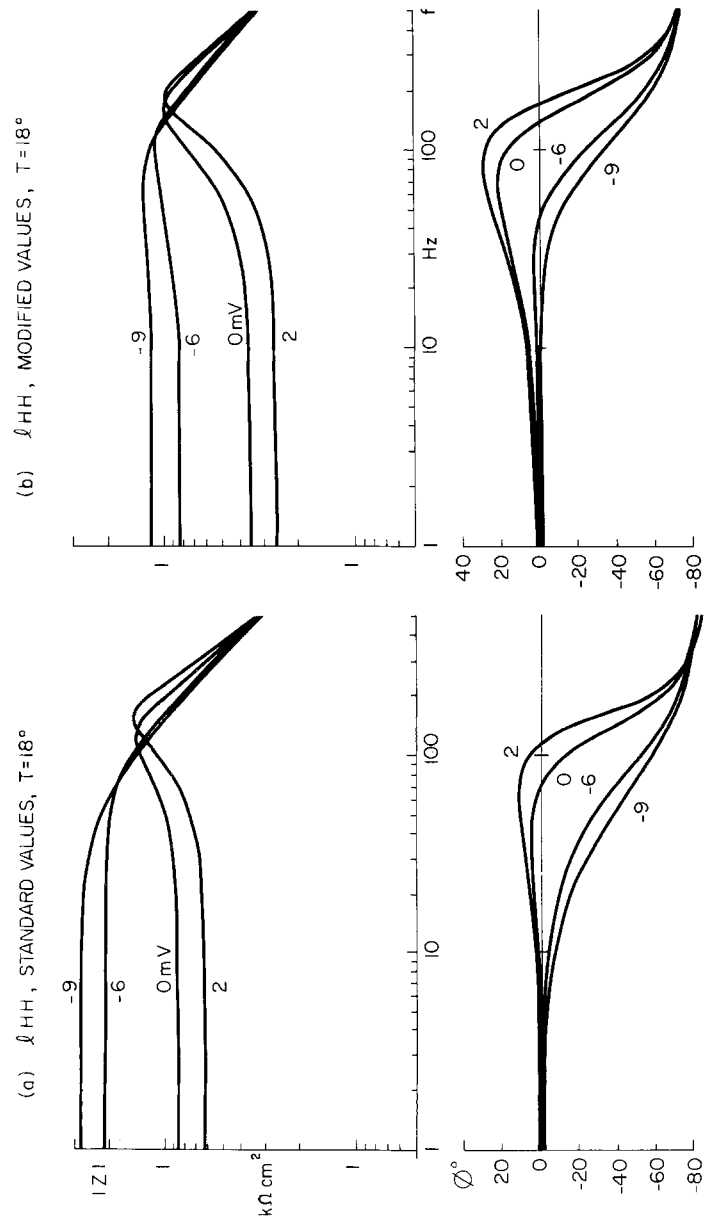

Fig. 14. Calculations of $|Z|$ and ϕ from the ℓHH equations for the same conditions of potential and temperature as the data in Fig. 8. (*a*) Standard *HH* values: $\bar{g}_K$ (36 mmho/cm^2), $V_K(-12$ mV), $\bar{g}_{Na}$ (120 mmho/cm^2), V_{Na} (115 mV), g_L (0.3 mmho/cm^2), V_L (10.6 mV), Q_{10} (3). (*b*) Modified values as follows: $\bar{g}_K$ (50 mmho/cm^2), $V_K(-22$ mV), g_L (0.6 mmho/cm^2), Q_{10} (2); all others are the same. Also a conductance of 143 mmho/cm^2 was assumed in series with the ℓHH membrane in these calculations

in squid axon were identical. They regarded this observation as evidence that the potassium concentration in the immediate vicinity of the membrane builds up after repetitive activity. The excess $[K_0^+]$, after activity, decayed in an exponential time course with a time constant of 30–100 msec. Frankenhaeuser and Hodgkin considered two possible explanations:

(1) a finite diffusion barrier in direct contact with the membrane (no space), and (2) a thin barrier to diffusion separated from the axon by a finite space. The former hypothesis is analogous to an unstirred diffusion layer which has been treated in detail by Neumcke (1971). They rejected (1) because it does not give an adequate description of the estimated excess $[K_0^+]$ build-up for short times. Furthermore, for short times, (1) predicts a decrease in the concentration proportional to $t^{-\frac{1}{2}}$ which would make the time course of the spike undershoot dependent on the rate at which K^+ diffuses away from the membrane (Frankenhaeuser & Hodgkin, 1956). More recent experiments by Adelman, Palti & Senft (1973) have supported interpretation (2). However, as suggested by Frankenhaeuser and Hodgkin, the data can be described by a combination of (1) and (2) if the dimensions of the space are altered.

For the purpose of the present discussion, a simplified and approximate circuit description of diffusion polarization was made by adding a parallel RC in series with the ℓHH membrane description as shown in the circuit in Fig. 15. An RC was chosen because it is, in fact, the circuit description for hypothesis (2), which introduces a compartment next to the membrane. For an applied steady-state membrane potential, K^+ current flows outward and increases $[K_0^+]$ in the compartment. The increase in $[K_0^+]$ follows an exponential time course (Frankenhaeuser & Hodgkin, 1956, Eq. 4) to give a steady-state condition. The increase in $[K_0^+]$ is equivalent to charging a capacitor in series with the membrane so that the effective driving force (transmembrane potential $- V_K$) is reduced with a time constant, which is the RC product. Alternatively, hypothesis (1) yields a time course which decays as $t^{-\frac{1}{2}}$ (Frankenhaeuser & Hodgkin, 1956, Eq. 10*a*; Neumcke, 1971, Eq. 28). A circuit synthesis of a $t^{-\frac{1}{2}}$ function can be achieved by a RC ladder network (Barnes & Jarvis, 1971). Thus a single RC may be considered to be a rough approximation of hypothesis (1) also.

Fig. 15 shows the result of computations of $|Z|$ and ϕ for a parallel RC in series with the ℓHH membrane. The corrected HH parameters were again used as in Fig. 14*b*, to give a better fit of the data. The computation was made for various values of R and C to produce curves which gave the best approximation to the data of Fig. 8. It appears that the inclusion of a series RC produces a low frequency feature which is qualitatively the same as the data. However, there is one important difference. The dip in $|Z|$ becomes more pronounced with increasing (less negative) potential and the intermediate zero phase crossing shifts to higher frequencies for the computations in Fig. 15. Potential change produces

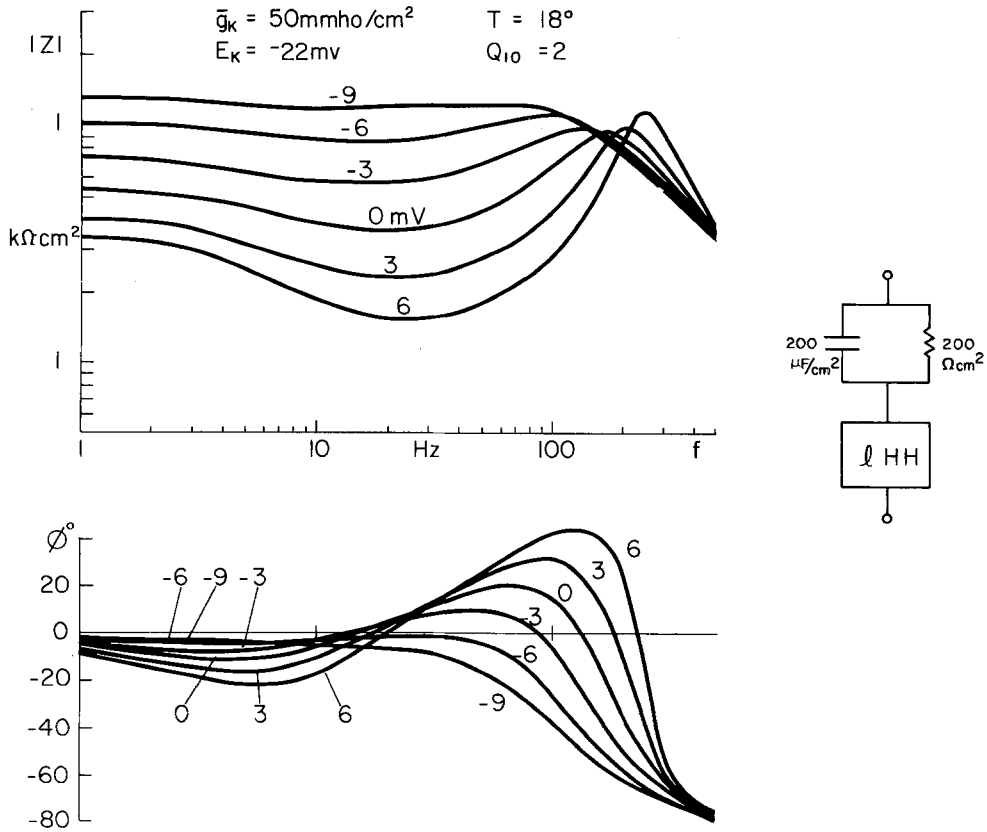

Fig. 15. Simulation of diffusion polarization effects in Schwann cell space about axon by computation of magnitude and phase of a parallel combination of fixed capacitance ($200\,\mu F/cm^2$) and resistance ($200\,\Omega \times cm^2$) in series with ℓHH membrane. With increasing depolarization, the dip in $|Z|$ becomes more pronounced, and the intermediate zero ϕ crossing of frequency axis shifts to higher frequencies, which is contrary to data in Figs. 8, 10, and 11

the opposite effects in the data (Fig. 8). There is an additional discrepancy. The data show positive phase at very low frequencies (1–2 Hz, Fig. 8, Fig. 10, Fig. 11) for some potentials. The computations, however, do not give a third zero phase crossing. That is, as frequency approaches zero, ϕ approaches, but does not cross, zero. Consequently, although this approximation of diffusion polarization can modify overall membrane conduction behavior to produce a low frequency dip in $|Z|$ and negative phase, the potential dependence and very low frequency behavior suggest that it does not give an adequate account of the data. Resolution of the problem is frustrated by the fact that $[K_0^+]$ accumulation depends upon K^+ current flow, and it is difficult to affect one without affecting the other. One possibility is to measure impedance for variations in $[K_i^+]$ and $[K_0^+]$

while maintaining the ratio $[K_0^+]/[K_i^+]$ constant. If the low frequency feature arises from an axon membrane property, the impedance should be invariant.

In conclusion, impedance and admittance measurements confirm the existence of a phenomenon associated with K^+ conduction which can produce peaking (sharp corners) in spontaneous current noise spectra (Fishman, Moore & Poussart, 1975). This result supports the assertion that a small area (patch) measurement of spontaneous fluctuations provides better resolution of spectral components than a large area measurement in squid axons (Fishman, Poussart & Moore, 1975). If the phenomenon is due to effects in the axon sheath, then the *HH* description of K^+ conduction in the excitable membrane is adequate, whereas if it is not attributable to diffusion polarization (as suggested by these experiments) the *HH* membrane K^+ conduction description is not correct. This point is critical for microscopic models. In any event, these measurements clearly indicate that the overall K^+ conduction kinetics in squid axon are not described by a single first order process and that, as suggested by Frankenhaeuser and Hodgkin (1956), the original *HH* formulation must be modified in order to accurately describe measured data from squid axons.

We thank Dr. Ronald D. Grisell and Mr. Paul D. Sawyer for computer assistance and Mr. William Law, Jr., for aid in instrumentation. This work was supported partially by NIH grants NS-11764 (HMF) and NS-80409 (LEM), and by Canadian National Research Council grant A 5274 (DJMP).

Note Added in Proof

Since submission of this paper, several related developments have occurred. Using a high-frequency admittance bridge, Takashima reported (*J. Membrane Biol.* **27**:21, 1976) that the total capacitance is frequency dependent and changes with polarizations from rest potential. From our low-frequency Z and Y measurements described here, it is clear that an overall capacitance measurement reflects not only the dielectric behavior of the membrane but also the voltage-dependent capacitive reactance (susceptance) of the Na conduction system (*see* Fig. 13) which is eliminated after application of TTX. Thus significant changes in capacitance with potential changes are expected due to a contribution from the reactive (susceptive) behavior of the Na conduction system. Changes in the dielectric portion of the membrane with potential are best interpreted from measurements in which the ion conduction systems have been suppressed. We have made complex admittance measurements under suppressed ion conduction conditions, during step voltage clamp, using a fast new method (Poussart, Moore, and Fishman, *Biol. Bull.* **151**:425, 1976). For depolarizing potential changes we find from admittance measurements a *decrease* in equivalent capacitance of 0.07 to 0.15 $\mu F/cm^2$, whereas the apparent capacitance, calculated from the difference between

current responses to paired depolarizing and hyperpolarizing step clamp pulses, gave a capacitance *increase* of 0.36 $\mu F/cm^2$. These measurements are reconciled only if "gating" current inactivates in steady state measurements at depolarized potentials. Finally, spontaneous fluctuations in Na conduction have been identified after suppression of K current and noise by internal perfusion with Cs or tetramethylammonium in squid axon (Fishman, Moore, and Poussart, *Biol. Bull.* **151**:408, 1976; Moore, Fishman, and Poussart, *Biophys. Soc.* (*Abstr.*), 1977).

References

Adelman, W.J., Jr., Palti, Y., Senft, J.P. 1973. Potassium ion accumulation in a periaxonal space and its effect on the measurement of membrane potassium ion conductance. *J. Membrane Biol.* **13**:387

Barnes, J.A., Jarvis, S., Jr. 1971. Efficient numerical and analog modelling of flicker noise processes. *Nat. Bur. Stand. Tech. Note* **604**

Bendat, J.S., Piersol, A.G. 1971. Random Data: Analysis and Measurement Procedures. Wiley-Interscience, New York

Brinley, F.J., Mullins, L.J. 1967. Sodium extrusion by internally dialyzed squid axons. *J. Gen. Physiol.* **50**:2303

Canessa-Fischer, M., Zambrano, F., Rojas, E. 1968. The loss and recovery of the sodium pump in perfused giant axons. *J. Gen. Physiol.* **51**:1625

Chandler, W.K., Fitzhugh, R., Cole, K.S. 1962. Theoretical stability properties of a space-clamped axon. *Biophys. J.* **2**:105

Cole, K.S. 1968. Membranes, Ions and Impulses. University of California Press, Berkeley

Conti, F., DeFelice, L.J., Wanke, E. 1975. Potassium and sodium ion current noise in the membrane of the squid giant axon. *J. Physiol.* (*London*) **248**:45

Davies, W.D.T. 1970. System Identification for Self-Adaptive Control. Wiley-Interscience, London

Fishman, H.M. 1970. Direct and rapid description of the individual ionic currents of squid axon membrane by ramp potential control. *Biophys. J.* **10**:799

Fishman, H.M. 1973. Low impedance capillary-electrode for wideband recording of membrane potential in large axons. *IEEE Trans. Biomed. Eng.* **20**:380

Fishman, H.M. 1973*a*. Relaxation spectra of potassium channel noise from squid axon membranes. *Proc. Nat. Acad. Sci. USA* **70**:876

Fishman, H.M. 1975. Rapid complex impedance measurements of squid axon membrane via input-output cross correlation function. *In*: Proceedings of First Symposium on Testing and Identification of Nonlinear Systems. G.D. McCann and P.Z. Marmarelis, editors. p. 257. California Institute of Technology, Pasadena

Fishman, H.M., Moore, L.E., Poussart, D.J.M. 1975. Potassium-ion conduction noise in squid axon membrane. *J. Membrane Biol.* **24**:305

Fishman, H.M., Moore, L.E., Poussart, D.J.M., Siebenga, E. 1976. Non first-order K^+ conduction impedance and noise feature in squid axon membrane. *Biophys. J.* **16**:26*a*

Fishman, H.M., Poussart, D.J.M., Moore, L.E. 1975. Noise measurements in squid axon membrane. *J. Membrane Biol.* **24**:281

Frankenhaeuser, B., Hodgkin, A.L. 1956. The after-effects of impulses in the giant nerve fibers of *Loligo*. *J. Physiol.* (*London*) **131**:341

Guttman, R., Feldman, L. 1975. White noise measurement of squid axon membrane impedance. *Biochem. Biophys. Res. Commun.* **67**:427

Guttman, R., Feldman, L., Lecar, H. 1974. Squid axon membrane response to white noise stimulation. *Biophys. J.* **14**:941

Kubo, R. 1957. Statistical-mechanical theory of irreversible processes. I. General theory and simple applications to magnetic and conduction problems. *J. Phys. Soc. Jpn.* **12**:570

Lee, T.W. 1960. Statistical Theory of Communication. Whiley, New York

Marmarelis, P.Z., Naka, K-I. 1974. Identification of multi-input biological systems. *IEEE Trans. Biomed. Eng.* **21**:88

Matsumoto, N., Inoue, I., Kishimoto, U. 1970. The electric impedance of the squid axon membrane measured between internal and external electrodes. *Jpn. J. Physiol.* **20**:516

Mauro, A., Conti, F., Dodge, F., Schor, R. 1970. Subthreshold behavior and phenomenological impedance of the squid giant axon. *J. Gen. Physiol.* **55**:497

Neumcke, B. 1971. Diffusion polarization at lipid bilayer membranes. *Biophysik* **7**:95

Nyguist, H. 1928. Thermal agitation of electric charge in conductors. *Phys. Rev.* **32**:110

Siebenga, E., Meyer, W.A., Verveen, A.A. 1973. Membrane shot-noise in electrically depolarized nodes of Ranvier. *Pfluegers Arch.* **341**:87

Takashima, S., Schwan, H.P. 1974. Passive electrical properties of squid axon membrane. *J. Membrane. Biol.* **17**:51

Takashima, S., Schwan, H.P., Cole, K.S. 1975. Membrane impedance of squid axon during hyperpolarization and depolarization. *Biophys. J.* **15**:39*a*

Takashima, S., Yantorno, R., Pal, N.C. 1975. Electrical properties of squid axon membrane. II. Effect of partial degradation by phospholipase A and pronase on electrical characteristics. *Biochim. Biophys. Acta* **401**:15

Taylor, R.E. 1965. Impedance of squid axon membrane. *J. Cell. Comp. Physiol.* **66** (*suppl.* 2):21